Noname manuscript No.
(will be inserted by the editor)

A. Montessori · G. Falcucci · M. La Rocca · S. Ansumali · S. Succi

Three-dimensional Lattice Pseudo-Potentials for Multiphase Flow Simulations at High Density Ratios

Received: date / Accepted: date

Abstract It is shown that the combination of generalized Van der Waals equations of state with high-order discrete velocity lattices, permits to simulate the dynamics of liquid droplets at air-water density ratios, with very moderate levels of spurious currents near the droplet interface. Satisfactory agreement with experimental data on droplet collisions at density ratios of order thousand is reported.

Keywords Multiphase flows · Lattice Boltzmann Models · Droplet collisions

1 Introduction

Lattice kinetic theory has attracted major interest in the last two decades, with major focus on in the simulation of a broad variety of complex flows, from fluid turbulence to transport in porous media and many others [28,1,

A. Montessori
Dept. of Engineering - University of Rome "Roma Tre"
Via della Vasca Navale 79, 00141 Rome - Italy
E-mail: and.montessori@gmail.com

G. Falcucci
Dept. of Engineering - University of Naples "Parthenope"
Centro Direzionale - Isola C4, 80149 Naples - Italy

S. Ansumali
Jawaharlal Nehru Centre for Advanced Scientific Reaserach,Engineering Mechanics Unit, Jakkur, Bangalore - 560064 Karnataka

M. La Rocca
Dept. of Engineering - University of Rome "Roma Tre"
Via della Vasca Navale 79, 00141 Rome - Italy

S. Succi
Istituto per le Applicazioni del Calcolo, CNR
Via dei Taurini 19, 00185 Rome - Italy

4]. In particular, lattice Boltzmann (LB) models for non-ideal fluids have known a major boost in connection with the simulation of complex multiphase and multicomponent flows [26]. **The main appealing feature of the method is its algorithmic simplicity. In particular, there is neither a need of tracking complex interfaces nor to solve the Poisson problem for the pressure, both being very computationally expensive tasks. The price to pay is small time steps to track the compressibility effects, as well as a diffuse interface, covering a few lattice sites.** As of today, many families of LB methods are available to simulate multiphase flows **[25,13,20,11]**, each with its own specific merits and weaknesses. Among others, the Shan-Chen (SC) pseudopotential model has gained a prominent role, mostly on account of its simplicity and flexibility. A major limitation of the Shan-Chen model, however, is that non-ideal interactions are encoded via a single-parameter attractive potential, acting on the first Brillouin region of the lattice. The result is that the equation of state and the surface tension cannot be varied independently. This limitation was lifted by extending the Shan-Chen formulation to the case of multi-range potential, acting upon two Brillouin regions **[10,9,21,24]**. These extensions have proved extremely fruitful, not only in terms of enhancing the numerical stability of the SC model, but also in terms of opening up a new set of applications, particularly the rheology of soft-glassy materials, such as foams and emulsions [3]. Another unphysical feature of the Shan-Chen model is a higher sound speed in the gas than in the liquid phase, which results from the lack of hard-core repulsion in the model. This problem has been circumvented by resorting to different families of equations of state (EoS), typically in the form of generalizations of the cubic Van Der Waals EoS [5,34]. **The numerical simulations presented in this paper suggest that** these two upgrades, multi-range lattice potentials and generalized VdW EoS, provide a significant boost in the numerical stability of the pseudo-potential method. In particular, they permit to simulate multiphase flows at air-water density ratios, while keeping numerical artifacts well below the physical signal.

2 Pseudo-potential model on higher-order lattices

2.1 The Lattice Boltzmann Equation with pseudo-potentials

The lattice Boltzmann (LB) equation with forcing terms reads as follows:

$$f_i(\mathbf{x}+\mathbf{c}_i\Delta t, t+\Delta t) - f_i(\mathbf{x},t) = -\omega\Delta t\,(f_i - f_i^{eq}) + F_i\Delta t \qquad (1)$$

where $f_i(\mathbf{x},t) \equiv f(\mathbf{x},\mathbf{v}=\mathbf{c}_i,t)$ is the discrete distribution function providing the probability of finding a particle at lattice site $\mathbf{x}$ at time t with discrete velocity $\mathbf{c}_i$, being $i=0,...,b$ the number of lattice directions, [19].
Eq.(1) describes the evolution of the discrete single-particle distribution function in terms of *streaming* (left hand side) and *collision*, in the form of a relaxation towards a local equilibrium (first term at right hand side). The local equilibria are computed as second-order expansion in the local Mach number, $\mathrm{Ma} = u/c_s$, u being the macroscopic flow velocity and c_s the lattice speed of sound, whose value has been set to 1/3:

$$f_i^{eq}(\mathbf{x},t) = w_i\rho\left(1 + \frac{\mathbf{u}\cdot\mathbf{c}_i}{c_s^2} + \frac{(\mathbf{u}\cdot\mathbf{c}_i)^2}{2c_s^4} - \frac{\mathbf{u}\cdot\mathbf{u}}{2c_s^2}\right) \tag{2}$$

where w_i are weights of the discrete equilibrium distribution functions and:

$$\rho(\mathbf{x},t) = \sum_i f_i(\mathbf{x},t) \tag{3}$$

$$\mathbf{u}(\mathbf{x},t) = \frac{\sum_i f_i(\mathbf{x},t)\mathbf{c}_i}{\rho(\mathbf{x},t)} \tag{4}$$

the fluid density and the flow velocity, respectively. The second term at the right hand side of Eq.(1) accounts for the effect of external/internal forces acting on the fluid molecules.

In the SC pseudo-potential scheme, the non-ideal force takes the form [25]:

$$\mathbf{F}(\mathbf{x},t) = -G\psi(\rho(\mathbf{x};t))\Delta t\sum_i p_i\mathbf{c}_i\psi(\rho(\mathbf{x}+\mathbf{c}_i\Delta t,t)) \tag{5}$$

where G is the strength of non-ideal interactions, p_i are the weights for the nth-isotropic lattice (see 2) and the *generalized density* $\psi(\rho)$ contributes the excess pressure in the non-ideal equation of state:

$$p = \rho c_s^2 + \frac{G}{2}\psi^2(\rho). \tag{6}$$

In the SC model, one has:

$$\psi(\rho) = 1 - e^{-\rho} \tag{7}$$

which gives a critical pressure $p_c = (ln2 - 1/2)/3 \sim 0.063$ and a critical coupling $G_c = -4$. We remind that negative G's code for attraction, the only interaction in the SC model. Note that in the ideal gas limit $\rho \to 0$, the SC EoS delivers $p = \rho c_s^2$, with a fixed sound speed $c_s^2 = 1/3$.

The Carnahan-Starling (CS) equation of state reads as follows [5]:

$$p = \rho v_T^2\,\frac{1 + r + r^2 - r^3}{(1-r)^3} - a\rho^2 \tag{8}$$

where $v_T = \sqrt{k_B T/m}$ is the thermal speed and a,b are the standard Van der Waals (VdW) parameters associated with the strength of long-range attraction and short-range repulsion. In the above, $r \equiv b\rho/4$.

The fluid critical temperature and pressure, respectively T_c and p_c, are controlled by the two interaction parameters, a and b, according to the relation:

$$T_c = 0.3773a/b, \;\; p_c = 0.0707a/b^2 \tag{9}$$

where the gas constant has been set to $R = 1$.

Based on Eq.(6), the CS generalized density is computed as:

$$\psi(\rho) = \sqrt{2\frac{p/c_s^2 - \rho}{G}}. \tag{10}$$

where the G is inserted only to ensure the positivity of the term under the square root [34]. As compared to the standard VdW, the CS equation is characterized by a steepening of the repulsive interactions in the hard-core region, which results in higher vapor/liquid density ratios at sufficiently high densities. We also note that the presence of a tunable thermal speed v_T in Eq.(8), instead of the fixed sound speed c_s in the SC EoS. By lowering the absolute temperature T at a given value of the reduced temperature T/T_c, it is therefore possible to implement weaker gradients on the vapor phase, as compared with the SC case. This feature is crucial for the stability of the vapor-liquid interface in the CS simulations [7].

Summarizing, the continuum limit of the above model recovers the quasi-incompressible Navier Stokes equations with the following pressure tensor:

$$\Pi_{a,b} = (\rho c_s^2 + G\frac{c_s^2}{2}\psi^2 + G\frac{c_s^4}{4}|\nabla\psi^2| + G\frac{c_s^4}{2}\psi\Delta\psi)\delta_{a,b} - \frac{1}{2}Gc_s^4\partial_a\psi\partial_b\psi \quad (11)$$

where ψ is given by Eq. 10 and the latin subscripts a,b refer to the spatial coordinates. With this definition, the surface tension is given by:

$$\sigma = -\frac{Gc_s^4}{2}\int_{-\infty}^{+\infty}|\partial_n\psi|^2 dn \quad (12)$$

where n denotes the normal to the interface.
In general this integral cannot be computed exactely and consequently the surface tension is numerically assessed via the Laplace test (see subsection 3.2). It is known that in pseudo-potential LB models the interface structure, density and velocity, transits from one phase to another driven by a non-ideal equation of state. This means that the bulk values of the density and velocity field across the interface are compliant with mechanical stability of the interface and the thermodynamic equation of state. In principle, in the presence of non-solenoidal forces ($\nabla \cdot \mathbf{F} \neq 0$)), there is a first order error in the continuity equation (see [11]). However, such an error can be cured by taking the velocity field as an average between the pre-collisional and post-collisional values [12] (See also [33,2]).

2.2 Discretisation of the non-ideal forcing term on higher-order lattices

Like any other diffuse-interface method, pseudo-potential multiphase models are affected by spurious currents, namely artificial recirculation patterns in the proximity of curved interfaces of stationary droplets, which arise as a result of the lack of symmetry of the underlying lattice [23,21].
Such spurious currents represent a serious tap to the numerical simulation of multiphase flows at substantial density ratios, since their magnitude is directly related to the ratio between the densities of the coexisting phases. For instance, spurious currents prevent the standard SC model from simulating flows at density ratios above $50 - 100$.

Hence, the search for methods and techniques to reduce their detrimental effects represents one of the leading themes of modern multiphase flow simulation [30,31,8,22,29]. Given their central role in lattice kinetic simulations of multiphase flows, a few additional comments on the implementation of pseudo-potential forces are in order.

By expanding the right-hand side of Equation (5) in Taylor series, we obtain (with $\Delta t = 1$ for simplicity):

$$\sum_i p_i \psi(\mathbf{x} + \mathbf{c}_i, t)\mathbf{c}_i = \nabla\psi \cdot E^{(2)} + \frac{1}{3!}\nabla^{(3)}\psi \cdot E^{(4)} + \frac{1}{5!}\nabla^{(5)}\psi \cdot E^{(6)} + ... \tag{13}$$

where the generic n^{th} order lattice tensor is defined as follows [32]:

$$E^{(n)} = \sum_i p_i (c_i)_{\alpha_1} \cdots (c_i)_{\alpha_n} \tag{14}$$

and Greek subscripts stand for the generic cartesian component x, y, z. The quality of the left-hand side of Equation (13) as an approximation of its continuum counterpart is strictly dictated by the degree of isotropy of the corresponding tensors $E^{(n)}$ [23]. For instance, with standard lattices, the best one can obtain is fourth-order isotropy, while two-Brillouin potentials permit to reach up to eighth order isotropy.
It is worth mentioning that, in this work, only the derivatives of the pseudo-potential are discretized on a 8th-order lattice while, the distribution functions evolve on a classical 27 speeds lattice. In actual practice, this requires the identification of the proper set of weights providing the highest isotropy degree consistent with the given lattice connectivity. These coefficients have been computed in previous publications [21]; however, to the best of our knowledge, they have never been implemented for the case of 8th-*order isotropic* potentials in *three* spatial dimensions.

The main parameters of the higher order lattice are reported in Tables 1 and 2.

A sketch of the 27 and 93 discrete velocity lattices used in this work is reported in Fig.1 while details of the procedure leading to higher-order forcing schemes are given in the Appendix .
Since the performance of the three-dimensional multiphase simulations with multirange potentials is very sensitive to data organization issues, in the sequel we provide further details on the numerical implementation.

2.3 Implementation of multispeed pseudo-potentials

The discrete velocities of each lattice have been grouped within shells of increasing energy, as reported in Table 2. This arrangement is crucial to design a flexible system of lattice vectors for the force computation and the optimization of the corresponding memory access [27]. Indeed, this data structure permits a seamless transition from one lattice to another, by simply switching on and off the velocities belonging to each energy shell.

Table 1 Weights of the isotropic $E^{(4)}$ (D3Q27F27) and $E^{(8)}(D3Q27F93)$ (see the text for the notation) lattices in three spatial dimensions. The numbers in brackets refer to the energy of the corresponding shell, c_i^2, the index i spanning the full set of discrete speeds. The degeneracy indicates the number of discrete speeds in the given energy shell.

Energy shell	$E^{(4)}$	$E^{(8)}$	Degeneracy
$p(1)$	16/216	448/15120	6
$p(2)$	4/216	240/15120	12
$p(3)$	1/216	96/15120	8
$p(4)$		50/15120	6
$p(5)$		16/15120	24
$p(6)$		8/15120	24
$p(8)$		1/15120	12

Table 2 Discrete energy-momentum relation for higher-order isotropic lattices. The cumulative index denotes the progressive number of discrete velocities up to the given energy shell. The symbol Π denotes all possible permutations, whose number is given by the degeneracy of the shell.

w $(e = \sum_i c^2)$	$\mathbf{c}_i$	degeneracy	cumulative index
$p(0)$	$\Pi(0,0,0)$	1	1
$p(1)$	$\Pi(1,0,0)$	6	7
$p(2)$	$\Pi(1,1,0)$	12	19
$p(3)$	$\Pi(1,1,1)$	8	27
$p(4)$	$\Pi(2,0,0)$	6	33
$p(5)$	$\Pi(2,1,0)$	24	57
$p(6)$	$\Pi(2,1,1)$	24	81
$p(8)$	$\Pi(2,2,0)$	12	93

At variance with previous implementations, the weights have been chosen in such a way as to ensure that the sound speed of the 93-speed lattice coincides exactly with the lattice sound speed of the fluid in the 27-speed lattice (see Appendix). Despite their highly technical nature, these details are of great practical relevance in terms of computational efficiency and flexibility of the computer program. Indeed, the flexibility of the data structure discussed above reflects into a very mild computational overhead in going from low-order to high-order lattices (we have run several simulations with intermediate lattices, not shown here). Typical performances data, referred to an AMD Opteron Server with a maximum memory bandwidth of $51.2GB/s$ per socket, are about 6.3 and 4.9 MLUPS (Million Lattice Updates Per Second) for the $D3Q27F27$ versus $D3Q27F93$ lattices, where the notation $DnQmFp$ denotes a n-dimensional lattice with m discrete velocities for the fluid and p discrete velocities for the force calculation.

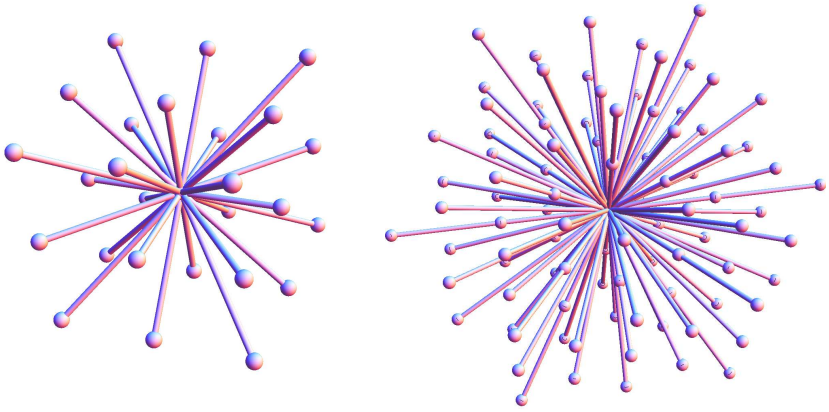

(a) (b)

Fig. 1 The set of discrete velocities for the the 4th- order 27-speeds (a) and of the 8th-order 93-speeds lattices (b).

3 Numerical Results

In order to assess the properties of the higher order lattice implementations with both SC and CS equations of state, we have run the standard phase-separation benchmarks and the Laplace tests. The maximum value of the spurious currents near the curved interfaces of the droplets has been monitored throughout the simulations. Furthermore, as a prospective application, we present a fully three-dimensional simulation of the off-axis grazing collision of two droplets in low density vapour ambient. It is found that the combination of the 93-speed lattice with the CS EoS permits to simulate liquid-vapor interfaces with density ratio over 1000 with very moderate spurious currents, i.e. well below the amplitude of the physical signal.

3.1 Coexistence curves

We simulate the coexistence of a liquid droplet within a vapour background, in order to asses the liquid-vapour curves for the $D3Q27F93$ lattice with the pseudo-potentials and the Carnahan-Starling equations of state. The simulation setup consists of a fully periodic cubic box of size 100^3, initialized with a liquid droplet of a given radius, placed in the center of the domain and surrounded by its vapour. The coexistence curves for different isotropic lattices are reported in Fig.2, which shows the values of the liquid-vapour density ratios as a function of the reduced temperature G/G_{cr} (SC) and T/T_{cr} (CS). A proper rescaling of the temperature-like parameter G is necessary in order to report both coexistence curves on the same plot. In particular, the values of the effective coupling parameter, G, for different density ratios can be

computed as follows:

$$G = -\frac{G_{cr}}{0.175}\left(\frac{T}{T_{cr}} - 1.75\right) \tag{15}$$

As one can see from Fig.2, the $D3Q27F27$ model with SC equation of state is stable for liquid density ratios up to approximately 700. Beyond this point, spurious currents trigger numerical instabilities. A density ratio of 700 marks a significant progress as compared to the standard SC implementation, which is typically limited to density ratios around 50. However, it should be observed that, at a density ratio 700, spurious currents are of the order of $U_{sp} \sim 0.3$, hence LB simulations with such large spurious currents would not be physically meaningful at low Mach numbers (i.e., since the speed of sound chosen here is $1/3$ and spurious currents are 0.3 Ma=0.9). Hence, even though they do not ruin the stability of the single droplet, the spurious currents are most likely to affect realistic multi-droplet simulations, in which the dynamics of a given droplet is influenced by the spurious wakes of other nearby droplets. Let us now comment on the CS coexistence curve. First, we note that up to $T/T_{cr} > 0.7$, the CS EoS provides a smaller density ratio than SC. However, below such value, the CS vapor branch goes below the SC one. In particular, at $T/T_{cr} \sim 0.61$, the SC runs unstable, while CS reaches up a density ratio of about 1000, with spurious currents of the order of 0.008, well below the typical LB flow speed, say $U = 0.1$. On the other hand, $D3Q27F27$ implementation of the CS EoS for the same density ratio, gives $U_{sp} \sim 0.045$, about five times the $D3Q27F93$ value. These results indicate that the benefits of the CS EoS versus SC are significantly enhanced by the 8-th order lattice. We wish to add that such functional dependency depend on the specific values of the attractive parameter a and might therefore be subject to further optimization. Moreover, in figure 2 the coexistence curve obtained with the present model is compared to that computed by means of the Maxwell construction for the same equation of state. As one can see, the results show good agreement for both the liquid and the vapour branch in a broad range of reduced temperature.

3.2 Laplace test and surface tension

In this section, we present the results of the standard Laplace tests. We recall that the Laplace law for a spherical droplet of radius R reads as follows:

$$\Delta P = \frac{2\sigma}{R} \tag{16}$$

where ΔP is the difference between inner and outer pressure in a spherical droplet of radius R and σ is the surface tension.
The surface tension is estimated by simulating a series of liquid droplets of various sizes, immersed in their vapour phase, and by measuring the values of both the liquid and vapour densities. As shown in Fig.4, the Laplace law holds to a good accuracy. Moreover, it should be noted that the surface tension can be lowered by decreasing the attractive parameter of the equation

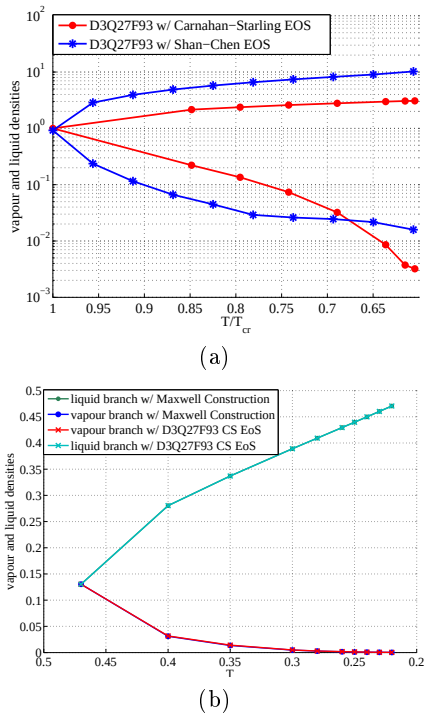

Fig. 2 (a) Spinodal decomposition with SC and CS EoS, with the 8th order lattice and the attraction parameter set to $a = 1$. The CS EoS allows to reach density ratios in excess of $1 : 1000$. (b) Comparison between the coexistence curves computed with the present model and those obtained by means of the Maxwell construction

of state. This lowering of the surface tension comes with an increase of the interface thickness (from 4 to 6 lattice points for $a = 1$ and $a = 0.5$ respectively) which, in turn, results in a sensible reduction of the maximum spurious currents at a given reduced temperature. In figure 3, the relation between the surface tension and the temperature of is compared against the Guggenheim-Katayama theoretical relation. It is evident that the two curves fit each other quite well thus representing a further proof of the consistency of the presented model to simulate complex multiphase flows at high density ratio.

3.3 Spurious currents

In this section, we report the effect of higher order lattice on the spurious currents for both SC and CS. In Fig.5, we report a systematic comparison between the maximum spurious currents around the droplet interface as a function the density ratio for the two equations of state. As expected the coupling between higher-order isotropic lattices and Van der Waals-like equation

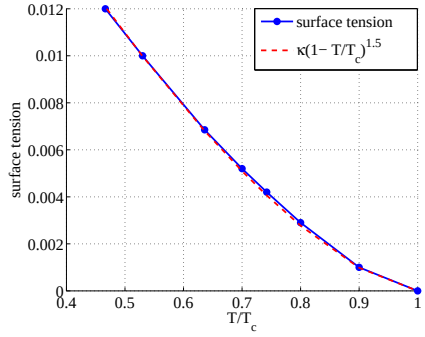

Fig. 3 Comparison between the present results and the Guggenheim-Katayama theoretical relation between the surface tension and the temperature.

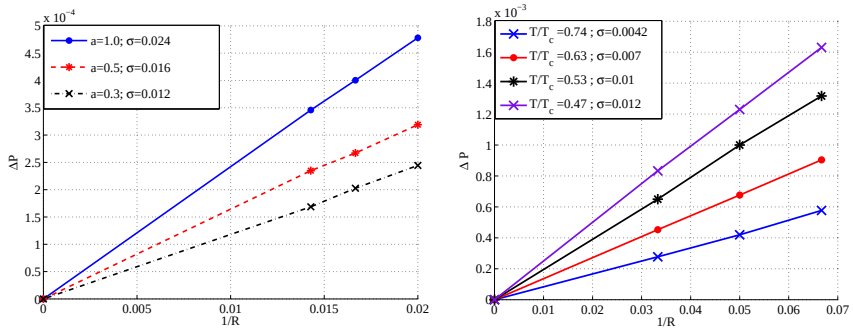

(a) (b)

Fig. 4 (a) and (b) Laplace test performed on a single liquid droplet with the 93-speed lattice for different temperatures and attractive parameters of the EoS. The use of different CS parameters, in particular $a = 1, 0.5, 0.3$ and $b = 1$, permits to change the value of the surface tension. In particular, changing a from $a = 1$ to $a = 0.3$, reduces the surface tension by a factor 2.

of state allows for a substantial reduction of the spurious currents near the droplet interface and, consequently, permits to simulate multiphase flows at density ratios above 1000.

3.4 Droplet off-axis binary collisions

As an application, we next present the case of a two-droplet off-axis collision at an impact parameter $\mathrm{I} \equiv Y/D = 0.68$, D being the diameter of the two droplets and Y the distance between the centers of the two droplets perpendicular to their relative velocity (see Fig.6). It is worth recalling that similiar simulations have been carried out previously, see for example [16,30, 17,14] By definition, $\mathrm{I} = 0$ denotes head-on collisions, while $\mathrm{I} \geq 1$ indicates no-collision at all. The main parameters are as follows: Reynolds number

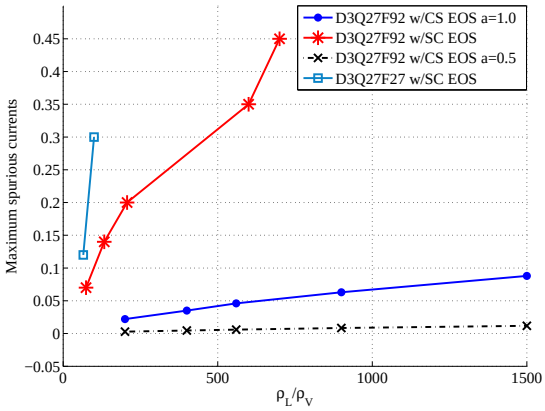

Fig. 5 Maximum spurious currents as a function of the density ratio for the SC and CS EoS, with 27 and 93-speed lattices. As known from the previous literature, the CS EoS allows a substantial reduction of the spurious currents, due to weaker gradients in the vapor phase, as compared to the SC case. Such benefits are significantly furthered by resorting to the 93-speed lattice with a suitably tuned value of the attraction parameter a. As one can see, going from $a = 1$ to $a = 0.5$ allows to further reduce the spurious currents by a factor $\simeq 7.5$, with respect to the case $a = 1$. To be noted that the benefits of the 93-speed lattice grow at increasing density ratioes. Use of the 93-speed lattice appears beneficial also for the SC case, in that it permits stable simulations at density ratios close to 700. However, at variance with the CS case, the SC spurious currents are very substantial, and consequently they are likely to affect the physical picture already at density ratios of the order of 100.

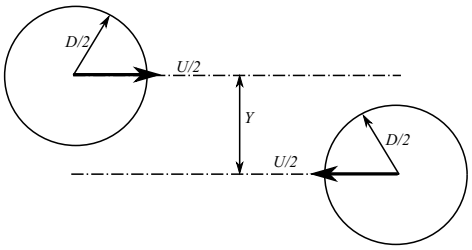

Fig. 6 Sketch of the off-axis collision between two droplets of radius $D/2$ with an initial velocity $U/2$.

$Re = UD/\nu \sim 313.7$, Weber number $We = \frac{\rho_l U^2 D}{\sigma} \sim 60.8$ and density ratio $\rho_L/\rho_V \sim 1000$, being ρ_l the density of the liquid phase and ρ_v the density of the vapour phase. In the fluid dynamic regime associated with the non-dimensional parameters given above, the droplets are expected to [18]:

a) merge, as they get close to each other;
c) stretch and form a ligament, due to their initial momentum along opposite (parallel) directions;
d) break-up the ligament, with a so-called end-pinching mechanism, due to their speed and momentum

e) separate again, at a small deflection angle, due to the large impact parameter, with the formation of multiple satellite droplets.

This is precisely the sequence of events emerging from the simulation, as reported in Fig.7, which refers to the following sequence of simulation time instants, $t = 0, 600, 1000, 1200, 1600, 2000, 2400, 3100, 3300$ (top-left to bottom-right). To be noted that, notwithstanding the large density ratio, the density contours appear very neat, with no sign of numerical debris at any stage of this complex evolution, including the "critical" stages of merging and rupture. Moreover the evolution of the collision process is visually compared with the experiments carried out by Qian and Law et. al [18]. The results are in good agreement, at least qualitatively. Indeed the kissing-like merging process and the consequent ligament stretching followed by the end-pinching mechanism are well captured by the simulation.

4 Further comments on discontinuity issues at the interface

Some authors have pointed out that multiphase LB models with emergent interfaces would suffer a discontinuity at the interface [11] because the continuity of mass momentum is defined only *implicitly* via the Maxwell area-rule, as combined with the conditions of mechanical instability of the interface. Leaving a detailed analysis of this issue for a future study, we have performed simulations of two-phase Poiseuille flow with planar interfaces and found excellent agreement with the analytical solutions, up to density ratios of the order 20. The bulk values of the density match the ones predicted by Maxwell's are-rule, with no appreciable sign of discontinuity of the tangential velocity (see Fig. 8). Beyond such density ratios, the method shows indeed a discontinuity of the tangential velocity at the interface, essentially due lack of resolution of the interface itself, about 5 lattice sites in our simulations. Larger jumps can be accomodated by thickening the interface, which can be achieved by lowering the surface tension. However, this comes with a tax in resolution and a corresponding penalty computational efficiency. A more efficient option might be offered by the combination of the present model with two-relaxation time or multi-time relaxation operators [15]. Based on the above, one might wonder whether the results at high density ratios, such as those presented in Fig. 7 would also be affected by such kind of issues. To this regard, we observe that the relevance of the multiphase Poiseuille test to the case of colliding droplets is far from being obvious, since the latter involves a *physical* sharp change of the tangential velocity across the interface, due to the droplet motion with respect to the surrounding fluid. Indeed, the reasonable agreement between our simulations and the experimental results highlighted in Fig. 7, seems to indicate that the issues of continuity raised by multiphase Poiseuille flows might be irrelevant to the case of moving droplets

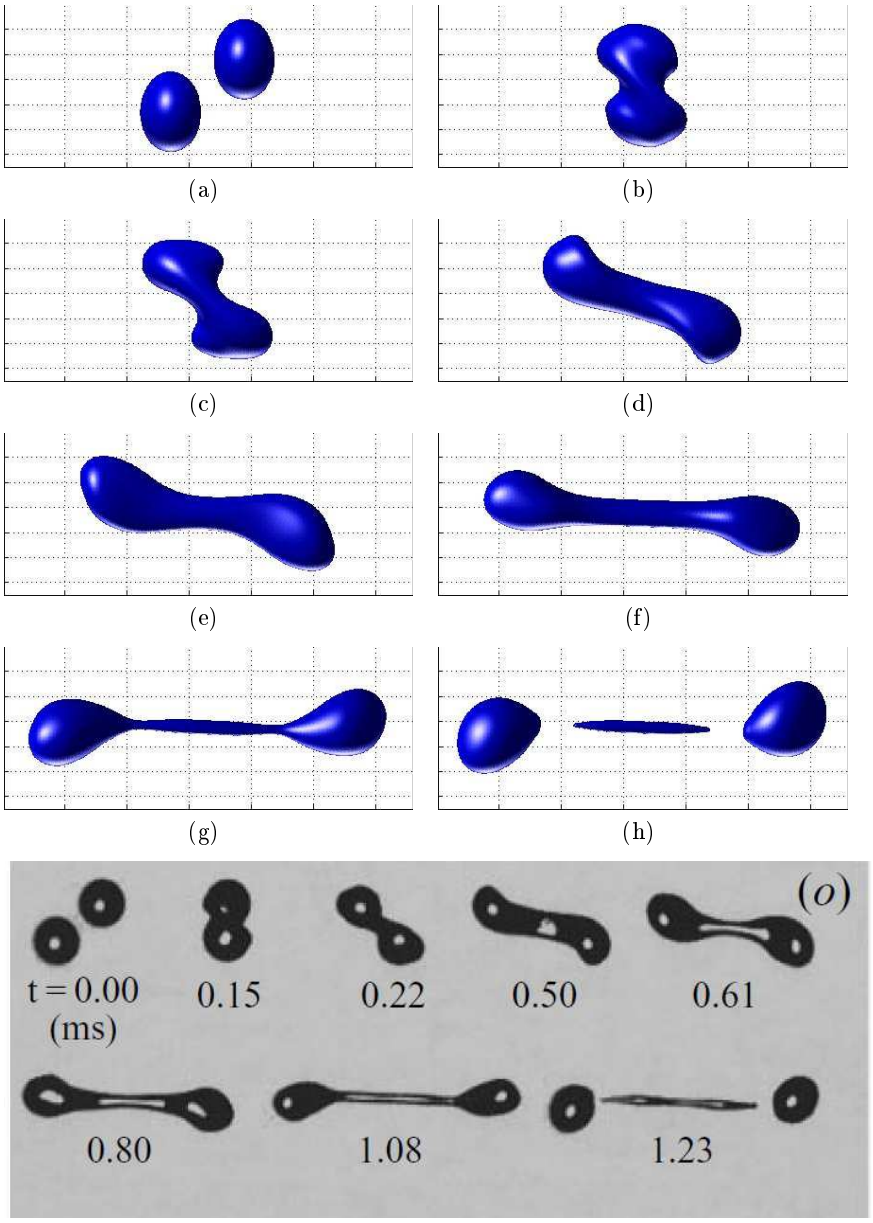

Fig. 7 Off-axis collision between two droplets. The droplets are impulsively started with an horizontal speed $U/2 = \mp 0.09$ towards the opposite side of the computational domain. The Weber and Reynolds number of the simulation are We $\simeq 60.8$ and Re $\simeq 313.7$ and the density ratio is about $1:1000$. The relaxation time is set to 0.62. The impact parameter is equal to 0.68 and the radius of the two droplet is set to 30 lattice points. The results are compared to those obtained by Qian and Law [18]. As one can see the evolution of the phenomenon is well captured by the numerical simulation. Indeed, as shown by the experiment, for this set of Reynolds and Weber, a kissing-like impact is performed after which a ligament appears that stretches and breaks up after an end-pinching mechanism.

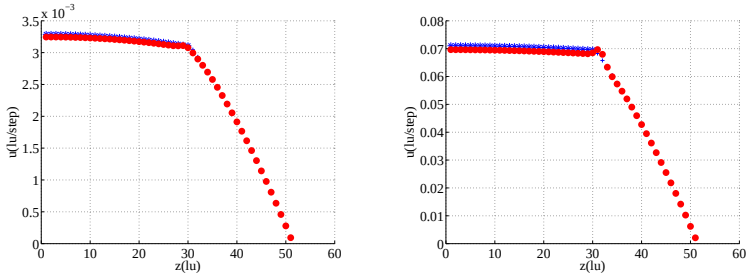

(a) (b)

Fig. 8 Tangential velocity profiles for the two-phase Poiseuille flow at density ratio (a) $\rho_L/\rho_V \sim 10$ and (b) $\rho_L/\rho_V \sim 25$, as compared to the analytical solution (crosses). The viscosity is set to $\nu = 1/6$ for both phases. In the figure lu stands for lattice units. The symbol u is the velocity component along the mainstream direction, while z is the crossflow coordinate.

away from solid walls. A deeper understanding of the above item, surely makes an important subject for future research.

5 Summary

Summarizing, we have shown that the implementation of the Carnahan-Starling equation of state, as combined with multi-range pseudo-potentials in high-order lattices with eighth order isotropy, permits to simulate multiphase flows at air-water density ratios, with spurious currents well below typical values of the flow speed in LB simulations. Satisfactory agreement between simulations and experimental data on off-axis droplet collisions has also been reported. It is hoped that these findings may help broadening the scope of lattice Boltzmann simulations of multiphase flows at high density ratios.

Acknowledgement

The research has been supported by the Italian national project "Hydroelectric energy by osmosis in coastal areas", PRIN 2010-2011.
Valuable discussions with M. Sbragaglia and R. Benzi are kindly acknowledged.

A Computation of the weights for higher-order lattices

Here we provide further details of the procedure leading to higher-order isotropic lattices in three dimensions up to a given order. The starting point in order to build up a nth-order isotropic lattice is to define a proper set of velocity vectors forming a regular and symmetric structure [6]. We consider cubic Bravais-like structures and define the generic $2n^{th}$-order isotropic lattice tensor as:

$$E^{(2n)}_{\alpha_1 \ldots \alpha_{2n}} = \sum_i p_i (c_i)_{\alpha_1} \cdots (c_i)_{\alpha_{2n}} \tag{17}$$

(odd-rank tensors are identically zero) and express it in terms of Kronecker deltas δ_{ij}. At this point, the problem of expressing the $2n^{th}$-rank tensor in terms of sums of products of Kronecker deltas can be cast in terms of combinatorial counting. Indeed, it can be shown that the generic $2n^{th}$-rank tensor consists of a sum of terms (in the form of Kronecker delta products) equal to:

$$\sum_i p_i (c_i^x)^{2l} (c_i^y)^{2m} (c_i^z)^{2p} = \kappa^{2n} (2l-1)!!(2m-1)!!(2p-1)!! \tag{18}$$

where $2l + 2m + 2p = 2n$ and $\kappa^{(2n)}$ is a constant. It is worth noting that, the discrete velocity set must satisfied the following two ansatz:

- Closure under Inversion
- Closure under Reflection

for further details please refer to [35].
We can now write a set of conditions which the lattice must obey in order to be isotropic at a given order:
1) Second-order isotropy:

$$\sum_i (c_i^x)^2 p_i = \sum_i (e_i^y)^2 p_i = \sum_i (c_i^z)^2 p_i = \kappa^2 \tag{19}$$

where $\kappa^{(2)}$ is equal to the square speed of sound.
2) Fourth-order:

$$\sum_i (c_i^x)^4 p_i = \sum_i (c_i^y)^4 p_i = \sum_i (c_i^z)^4 p_i = 3\kappa^4 \tag{20}$$

$$\sum_i (c_i^x)^2 (c_i^y)^2 p_i = \kappa^4 \tag{21}$$

the fourth-order isotropy condition can be written in a more compact form as:

$$\frac{\sum_i (c_i^x)^4 p_i}{\sum_i (c_i^x)^2 (c_i^y)^2 p_i} = 3 \tag{22}$$

3) Sixth-order isotropy:

$$\sum_i (c_i^x)^6 p_i = 15\kappa^6 \tag{23}$$

$$\sum_i (c_i^x)^4 (e_i^y)^2 p_i = 3\kappa^6 \tag{24}$$

$$\sum_i (c_i^x)^2 (c_i^y)^2 (c_i^z)^2 p_i = \kappa^6 \tag{25}$$

Above, the greek indices stand for the cartesian coordinates. In this case we can define three different conditions namely :

$$\frac{\sum_i (c_i^x)^6 p_i}{\sum_i (c_i^x)^4 (c_i^y)^2 p_i} = 5 \tag{26}$$

$$\frac{\sum_i (c_i^x)^6 p_i}{\sum_i (c_i^x)^2 (c_i^y)^2 (c_i^z)^2 p_i} = 15 \tag{27}$$

$$\frac{\sum_i (c_i^x)^4 (c_i^y)^2 p_i}{\sum_i (c_i^x)^2 (c_i^y)^2 (c_i^z)^2 p_i} = 3 \tag{28}$$

3) Eight-order isotropy:
in this case, the following four conditions apply :

$$\sum_i (c_i^x)^8 p_i = 105\kappa^8 \tag{29}$$

$$\sum_i (c_i^x)^6 (c_i^y)^2 p_i = 15\kappa^8 \tag{30}$$

$$\sum_i (c_i^x)^4 (c_i^y)^4 p_i = 9\kappa^8 \tag{31}$$

$$\sum_i (c_i^x)^4 (c_i^y)^2 (c_i^z)^2 p_i = 3\kappa^8 \tag{32}$$

References

1. Aidun, C., Clausen, J.: Lattice-boltzmann method for complex flows. Annual Review of Fluid Mechanics **42**, 439–472 (2010)
2. Benzi, R., Biferale, L., Sbragaglia, M., Succi, S., Toschi, F.: Mesoscopic modeling of a two-phase flow in the presence of boundaries: the contact angle. Physical Review E **74**(2), 021,509 (2006)
3. Benzi, R., Sbragaglia, M., Succi, S., Bernaschi, M., Chibbaro, S.: Mesoscopic lattice boltzmann modeling of soft-glassy systems: theory and simulations. The Journal of Chemical Physics **131**(10), 104,903 (2009)
4. Benzi, R., Succi, S., Vergassola, M.: The lattice boltzmann equation: theory and applications. Physics Reports **222**(3), 145–197 (1992)
5. Carnahan, N.F., Starling, K.E.: Equation of state for nonattracting rigid spheres. The Journal of Chemical Physics **51**(2), 635–636 (1969)
6. Chen, H., Goldhirsch, I., Orszag, S.A.: Discrete rotational symmetry, moment isotropy, and higher order lattice boltzmann models. Journal of Scientific Computing **34**(1), 87–112 (2008)
7. Colosqui, C.E., Falcucci, G., Ubertini, S., Succi, S.: Mesoscopic simulation of non-ideal fluids with self-tuning of the equation of state. Soft matter **8**(14), 3798–3809 (2012)
8. Ding, H., Spelt, P.D., Shu, C.: Diffuse interface model for incompressible two-phase flows with large density ratios. Journal of Computational Physics **226**(2), 2078–2095 (2007)
9. Falcucci, G., Bella, G., Chiatti, G., Chibbaro, S., Sbragaglia, M., Succi, S.: Lattice boltzmann models with mid-range interactions. Communications in Computational physics **2**, 1071–1084 (2007)
10. Falcucci, G., Ubertini, S., Succi, S.: Lattice boltzmann simulations of phase-separating flows at large density ratios: the case of doubly-attractive pseudo-potentials. Soft Matter **6**(18), 4357–4365 (2010)
11. Ginzburg, I.: Lattice boltzmann modeling with discontinuous collision components: Hydrodynamic and advection-diffusion equations. Journal of Statistical Physics **126**(1), 157–206 (2007)
12. Guo, Z., Zheng, C., Shi, B.: Discrete lattice effects on the forcing term in the lattice boltzmann method. Physical Review E **65**(4), 046,308 (2002)
13. He, X., Doolen, G.D.: Thermodynamic foundations of kinetic theory and lattice boltzmann models for multiphase flows. Journal of Statistical Physics **107**(1-2), 309–328 (2002)
14. Inamuro, T., Tajima, S., Ogino, F.: Lattice boltzmann simulation of droplet collision dynamics. International journal of heat and mass transfer **47**(21), 4649–4657 (2004)
15. Kuzmin, A., Mohamad, A., Succi, S.: Multi-relaxation time lattice boltzmann model for multiphase flows. International Journal of Modern Physics C **19**(06), 875–902 (2008)

16. Pan, Y., Suga, K.: Numerical simulation of binary liquid droplet collision. Physics of Fluids (1994-present) **17**(8), 082,105 (2005)
17. Premnath, K.N., Abraham, J.: Simulations of binary drop collisions with a multiple-relaxation-time lattice-boltzmann model. Physics of Fluids (1994-present) **17**(12), 122,105 (2005)
18. Qian, J., Law, C.: Regimes of coalescence and separation in droplet collision. Journal of Fluid Mechanics **331**, 59–80 (1997)
19. Qian, Y., d'Humières, D., Lallemand, P.: Lattice bgk models for navier-stokes equation. EPL (Europhysics Letters) **17**(6), 479 (1992)
20. Rothman, D.H., Keller, J.M.: Immiscible cellular-automaton fluids. Journal of Statistical Physics **52**(3-4), 1119–1127 (1988)
21. Sbragaglia, M., Benzi, R., Biferale, L., Succi, S., Sugiyama, K., Toschi, F.: Generalized lattice boltzmann method with multirange pseudopotential. Physical Review E **75**(2), 026,702 (2007)
22. Scardovelli, R., Zaleski, S.: Direct numerical simulation of free-surface and interfacial flow. Annual review of fluid mechanics **31**(1), 567–603 (1999)
23. Shan, X.: Analysis and reduction of the spurious current in a class of multiphase lattice boltzmann models. Physical Review E **73**(4), 047,701 (2006)
24. Shan, X.: Pressure tensor calculation in a class of nonideal gas lattice boltzmann models. Physical Review E **77**(6), 066,702 (2008)
25. Shan, X., Chen, H.: Lattice boltzmann model for simulating flows with multiple phases and components. Physical Review E **47**(3), 1815 (1993)
26. Shan, X., Chen, H.: Simulation of nonideal gases and liquid-gas phase transitions by the lattice boltzmann equation. Physical Review E **49**(4), 2941 (1994)
27. Shet, A.G., Sorathiya, S.H., Krithivasan, S., Deshpande, A.M., Kaul, B., Sherlekar, S.D., Ansumali, S.: Data structure and movement for lattice-based simulations. Physical Review E **88**(1), 013,314 (2013)
28. Succi, S.: The lattice Boltzmann equation: for fluid dynamics and beyond. Oxford university press (2001)
29. Sui, Y., Ding, H., Spelt, P.D.: Numerical simulations of flows with moving contact lines. Annual Review of Fluid Mechanics **46**, 97–119 (2014)
30. Tryggvason, G., Bunner, B., Esmaeeli, A., Juric, D., Al-Rawahi, N., Tauber, W., Han, J., Nas, S., Jan, Y.J.: A front-tracking method for the computations of multiphase flow. Journal of Computational Physics **169**(2), 708–759 (2001)
31. Tryggvason, G., Scardovelli, R., Zaleski, S.: Direct numerical simulations of gas–liquid multiphase flows. Cambridge University Press (2011)
32. Wolfram, S.: Cellular automaton fluids 1: Basic theory. Journal of Statistical Physics **45**(3-4), 471–526 (1986)
33. Xi, H., Duncan, C.: Lattice boltzmann simulations of three-dimensional single droplet deformation and breakup under simple shear flow. Physical Review E **59**(3), 3022 (1999)
34. Yuan, P., Schaefer, L.: Equations of state in a lattice boltzmann model. Physics of Fluids (1994-present) **18**(4), 042,101 (2006)
35. Yudistiawan, W.P., Kwak, S.K., Patil, D., Ansumali, S.: Higher-order galilean-invariant lattice boltzmann model for microflows: Single-component gas. Physical Review E **82**(4), 046,701 (2010)